ATP Consumption and Efficiency of Human Single Muscle Fibers with Different Myosin Isoform Composition

Zhen-He He,* Roberto Bottinelli,† Maria A. Pellegrino,† Michael A. Ferenczi,* and Carlo Reggiani†‡
†Institute of Human Physiology, University of Pavia, 27100 Pavia, Italy; ‡Department of Anatomy and Physiology, University of Padova, 35131 Padova, Italy; and *National Institute for Medical Research, London NW7 1AA, United Kingdom

ABSTRACT Chemomechanical transduction was studied in single fibers isolated from human skeletal muscle containing different myosin isoforms. Permeabilized fibers were activated by laser-pulse photolytic release of 1.5 mM ATP from p^3-1-(2-nitrophenyl)ethylester of ATP. The ATP hydrolysis rate in the muscle fibers was determined with a fluorescently labeled phosphate-binding protein. The effects of varying load and shortening velocity during contraction were investigated. The myosin isoform composition was determined in each fiber by sodium dodecyl sulfate-polyacrylamide gel electrophoresis. At 12°C large variations (three- to fourfold) were found between slow and fast (2A and 2A-2B) fibers in their maximum shortening velocity, peak power output, velocity at which peak power is produced, isometric ATPase activity, and tension cost. Isometric tension was similar in all fiber groups. The ATP consumption rate increased during shortening in proportion to shortening velocity. At 12°C the maximum efficiency was similar (0.21–0.27) for all fiber types and was reached at a higher speed of shortening for the faster fibers. In all fibers, peak efficiency increased to ~0.4 when the temperature was raised from 12°C to 20°C. The results were simulated with a kinetic scheme describing the ATPase cycle, in which the rate constant controlling ADP release is sensitive to the load on the muscle. The main difference between slow and fast fibers was reproduced by increasing the rate constant for the hydrolysis step, which was rate limiting at low loads. Simulation of the effect of increasing temperature required an increase in the force per cross-bridge and an acceleration of the rate constants in the reaction pathway.

INTRODUCTION

Skeletal muscle fibers are specialized to perform distinct functional tasks. Some fibers, which only shorten at low speed and develop modest power, have the advantage of consuming little energy for their contractile activity. Such fibers are used for the maintenance of posture. Other fibers shorten faster and develop greater power, but they are more energetically expensive. They provide the power for rapid, short-lasting movement. This functional specialization finds its molecular explanation in the presence of different myosin isoforms. Our intention here is to understand the biochemical mechanisms that account for the difference in contractile characteristics between fibers containing the various myosin isoforms.

In the last few years, the analysis of the molecular composition and of the contractile and energetic properties of the same short segments of skinned muscle fibers has made it possible to relate the functional and molecular diversity of skeletal muscle fibers. Myosin heavy chain (MHC) isoforms determine the maximum shortening velocity (e.g., Reiser et al., 1985; Bottinelli et al., 1991, 1996), peak mechanical power and optimal velocity for shortening (Bottinelli et al., 1991, 1996), ATP consumption rate during isometric contraction, and tension cost (Bottinelli et al., 1994; Stienen et al., 1996). Thus the myosin isoforms largely determine the contractile properties of muscle cells that allow them to adapt to the requirements for muscular performance in vivo according to functional demand.

However, much less is known about the energy consumption during shortening and therefore about the conversion of chemical energy into mechanical work and the efficiency of this process. Whereas it is clear that myosin isoforms are motors able to produce variable power with variable energy consumption, the link between power, energy, consumption, and efficiency is not well understood. Moreover, the study of the distinctive functional and biochemical properties of myosin isoforms has remained mainly descriptive in nature, despite significant contributions toward an understanding of the diversity in terms of cross-bridge cycle and actin-myosin interactions (Barclay et al., 1993; Potma and Stienen, 1996, Zhao and Kawai, 1994; Wang and Kawai, 1997). Here we determined ATP consumption during active shortening in single skeletal muscle fibers containing different myosin isoforms. This allowed calculation of the thermodynamic efficiency, of the distance traveled per ATP, and of the duty ratio, the fraction of time myosin heads remain attached to actin during contraction and shortening (Irving and Woledge, 1981) for two distinct myosin isoforms.

The difference in energy consumption between slow and fast muscle fibers during active shortening has mainly been studied in intact muscles of small mammals (mouse, rat, and rabbit), by indirect approaches such as oxygen consumption (Heglund and Cavagna, 1987) or heat production (Gibbs and Gibson, 1972; Wendt and Gibbs, 1973; Barclay et al., 1993; Holroyd et al., 1996). The only direct determination

Received for publication 18 November 1999 and in final form 7 April 2000.
Address reprint requests to Dr. Michael A. Ferenczi, National Institute for Medical Research, The Ridgeway, Mill Hill, London NW7 1AA, UK. Tel.: 0044-208-959-3666, ext. 2077; Fax: 0044-208-906-4419; E-mail: michael.ferenczi@nimr.mrc.ac.uk.

0006-3495/00/08/945/17 $2.00

of ATP consumption during shortening in isolated single fibers of known MHC isoform composition was made in skinned fibers of the rat by measuring the rate of change of NADH absorbance in an enzyme-linked assay (Reggiani et al., 1997). The results have shown that type 2B fibers develop much more power (sevenfold) than type 1 fibers with only slightly lower (−30%) efficiency. However, time limitations mainly caused by diffusion delay prevented determination of ATP consumption during shortening at the highest shortening velocities.

In this study the ATPase assay method of He et al. (1997, 1998a,b, 1999) was used to compare, during active shortening, the ATP consumption and efficiency of human muscle fibers containing various MHC isoforms. The method is based on the engineering of a high-affinity phosphate-binding protein of bacterial origin that is labeled with a coumarin fluorophore (Brune et al., 1994, 1998) and displays, under assay conditions, a fivefold increase in fluorescence upon phosphate binding. ATP hydrolysis was observed with a delay of less than 10 ms and micromolar resolution at shortening velocities ranging from nearly isometric conditions to almost V_{max}, the shortening velocity at zero load. Human muscle fibers were used because of their relevance to the study of human performance, aging, and disease and because their relatively slow kinetic properties (Stienen et al., 1996) make their study easier than that of muscle fibers obtained from smaller animal species. The ATPase of human fibers is sufficiently slow during maximum activation at optimal sarcomere length to allow its measurement at 12°C and at 20°C. As shown in previous studies, human muscle fibers are large, are stable in vitro after permeabilization, and maintain a good sarcomere pattern, even during repeated, long, maximum contractions (Larsson and Moss, 1993; Bottinelli et al., 1996). In addition, their MHC isoforms can be determined easily and unambiguously by gel electrophoresis (Biral et al., 1988; Stienen et al., 1996).

We show here that slow and fast human fibers have similar efficiencies despite the large difference in power output and energy consumption rate and that their efficiency increases with temperature. The results and their modeling also support the view that the dynamic differences between fast and slow human MHCs are most simply accounted for by a difference in the kinetic parameters of the actomyosin ATPase cycle.

MATERIALS AND METHODS

Muscle fibers

Surgical biopsies were obtained from the leg muscles (vastus lateralis and tibialis anterior) of two male subjects (age 30–50 years) with local anesthesia. The study was approved by the ethics committee of the Department of Medicine of the University of Genoa, Italy, and informed consent was obtained. Single fiber segments were dissected from the biopsy samples while they were immersed in ice-cold skinning solution, as previously described (Bottinelli et al., 1996; Stienen et al., 1996). The ends of the segments were attached to aluminum foil T-shaped clips and cross-linked with glutaraldehyde to reduce the compliance of the attachment regions (Chase and Kushmerick, 1988; Thirlwell et al., 1994; He et al., 1997, 1998b), leaving a 2–3-mm-long central, active region.

Fiber segments were transferred to the setup, where their contractile and energetic parameters were measured (see below). At the end of the experiment each fiber segment was placed in a small test tube containing 20 μl of Laemmli solution (Laemmli, 1970). MHC isoforms were separated by sodium dodecyl sulfate-polyacrylamide gel electrophoresis with 6% acrylamide, as described by Stienen et al. (1996). Three isoforms (MHC-1 or slow, MHC-2A, and MHC-2X) were separated. Four types of fibers were identified, depending on the presence of one or two MHC isoforms.

Experimental apparatus

The setup was described in detail in previous papers (He et al. 1997, 1999). Briefly, six 20-μl troughs were cut into a circular, stainless steel, temperature-controlled rotating block placed on the stage of a Zeiss ACM microscope (Oberkochen, Germany). The fiber was mounted horizontally between two hooks, which emerged through slits in the ends of the troughs. One hook was connected to a force transducer (AE 801; Sensonor, Horten, Norway), and the other to an electromagnetic puller. Surface tension prevented the solution from leaking out of the ends of the troughs. Five of the six troughs contained the incubating solutions. The last trough contained low-viscosity silicone fluid and had a fused silica front window to allow illumination of the fiber by light pulses from a frequency-doubled ruby laser used for the rapid photorelease of ATP by photolysis of NPE-caged ATP (P^3-1-(2-nitrophenyl)ethyl ester of ATP). The light pulses from the frequency-doubled, Q-switched ruby laser (Lumonics, Rugby, UK; 30 ns long, 50–100 mJ/pulse at a wavelength of 347 nm) were adjusted with a fused silica cylindrical lens to illuminate the whole length of the fiber segment in the horizontal plane. A single laser pulse caused the photolytic release of 1.5 mM ATP in a fiber preincubated with 5 mM NPE-caged ATP and immersed in silicone fluid, as determined previously (He et al., 1997).

Phosphate-binding protein and ATPase measurements

ATPase activity was calculated from the change in fluorescence of the phosphate-sensitive fluorescent protein MDCC-PBP diffused into the muscle fiber. The phosphate binding protein (PBP) was labeled with a coumarin fluorophore, *N*-(2-[1-maleimidyl]ethyl)-7-diethylamino-coumarin-3-carboxamide (MDCC), as described previously (Brune et al., 1994, 1998). The 400-μm-long center section of the fiber segment was illuminated at 420 nm through the 40× objective with the light from a tungsten lamp mounted in the epifluorescence port on the ACM microscope, as described previously (He et al., 1997, 1998a,b). Background fluorescence was low because the muscle fiber was immersed in silicone fluid during these measurements, so that the water-soluble fluorescent compound (MDCC-PBP) was confined to the volume of the fiber. Fluorescence was collected by the objective, and its intensity at 470 nm was measured by a photomultiplier tube mounted on the microscope head. Calibration procedures as well as the sensitivity and linearity of the measurements were described previously (He et al., 1997).

The concentration of inorganic phosphate (P_i) and hence the rate of P_i release were derived from the fluorescence signal after subtraction of the fluorescence background, recorded during a period before the laser pulse. The concentration of P_i released in the fiber was related to the amplitude of the fluorescence signal by

$$[P_i] = (F_t - F_{min}) \times [\text{MDCC-PBP}]/(F_{max} - F_{min}) \qquad (1)$$

where $[P_i]$ was the concentration of P_i (in mM) released in the fiber and bound to MDCC-PBP, [MDCC-PBP] indicated the concentration (in mM)

of the phosphate binding protein, F_t was the amplitude of the fluorescence signal at time t, F_{min} was the fluorescence signal before photolytic release of ATP, and F_{max} was the fluorescence signal when all of the MDCC-PBP was saturated with P_i. F_t, F_{min}, and F_{max} were in arbitrary units, which in practice were the photomultiplier tube current converted to voltage after amplification. The ATPase rate was derived from the gradient of fluorescence signal calibrated in terms of P_i concentration.

A light artifact on the fluorescence recordings caused by the pulse of laser light was followed by a further artifact that was caused by a short-lived *aci*-nitro intermediate formed as an intermediate of NPE-caged ATP photolysis that absorbed light at 420 nm (Corrie et al., 1992). At 12°C, the *aci*-nitro intermediate decayed with a rate constant of ~50 s^{-1} (He et al., 1998a). The fluorescence traces after photolysis were corrected by adding to the signal a rising exponential process with a rate constant of 50 s^{-1} starting at the time of the laser pulse, with an amplitude adjusted so that the lowest value for the fluorescence signal after correction was equal to the average of the fluorescence signal before photolysis (He et al., 1998b). The mean amplitude of the *aci*-nitro signal correction corresponded to 0.130 ± 0.005 mM P_i (n = 41) in the fluorescence signal, ~10% of the total fluorescence change.

A geometrical artifact accompanied fiber shortening. As the volume of the myofilament lattice is relatively constant, shortening was associated with an increase in cross-sectional area. Thus, during shortening the volume of fiber illuminated by the tungsten lamp increased and caused an increase in the emitted light. This increase was directly tested and measured by shortening the fiber at rest (He et al., 1999). To take this into account, the increase in fluorescence due to the volume increase was calculated and subtracted from the measured value of fluorescence (<5% correction; see He et al., 1999).

Sarcomere length measurements

The fiber was illuminated with the beam from a He-Ne laser over a length of ~0.5 mm to obtain diffraction orders produced by the sarcomere striations. The first-order diffracted beam was focused onto one of two position-sensitive photodiodes. The ratio of the difference to the sum of the output signals was used in the measurements as it varies linearly with the position of the centroid of the light falling on the diode.

At the beginning of the experiment the photodiode signal was adjusted to zero, and the calibration was obtained by recording the photodiode signal in response to movements of the photodiode that simulate the change in the angle of the first-order beam. The sarcomere signal often deteriorated during contraction and particularly during the shortening phase. The degradation of the signal was monitored from the fall of the intensity of the summed output of the photodiode (He et al., 1999).

Experimental protocol

Each muscle fiber was transferred from the dissecting stage to the setup and placed in a trough containing relaxing solution. The sarcomere length was adjusted to 2.6 μm, and the width and depth of the fiber were measured using the water immersion objective. The cross-sectional area was calculated from the length and width, assuming an elliptical shape. The length of the central region (between the two end regions exposed to glutaraldehyde) was measured.

The fiber was incubated for 30 min in relaxing solution containing 1% (v/v) Triton X-100 and then was washed twice in relaxing solution, and the sarcomere length was checked again. The sarcomere diffraction signal was optimized, and a sarcomere length calibration was obtained as described above. The fiber was transferred for 5 min into calcium-containing rigor solution. This rigor solution also contained purine nucleoside phosphorylase and 7-methyl guanosine, a "P_i mop," to reduce contaminating P_i (see He et al., 1997, for composition) and then was transferred for 7–10 min to a trough filled with loading solution (pH 7.1, ionic strength 150 mM adjusted with K-propionate and containing 32 μM free Ca^{2+}, 20 mM EGTA, 1 mM free Mg^{2+}, 20 mM glutathione, 60 mM 2-(*N*-tris[hydroxymethyl]methyl-2-amino)ethane sulfonic acid, 5 mM NPE-caged ATP, 1.2 mM P_i-free MDCC-PBP, and the ATP-regenerating system consisting of 4 mg/ml creatine kinase and 10 mM creatine phosphate) (He et al., 1997, 1999).

Finally the fiber was transferred to the trough containing silicone fluid. The epifluorescence head of the microscope was lowered so that the objective made contact with the silicone fluid and the shutter for the fluorescence excitation light was opened. A few seconds later, a pulse of near-UV laser light illuminated the fiber to induce contraction by the photolytic release of ATP from NPE-caged ATP. At a predetermined time after photolysis an electrical signal was applied to the motor controller to cause shortening of the muscle fiber. The extent of movement was fixed at 180 μm, corresponding to 7–9% fiber length. The applied velocity of shortening varied from zero to 1.2 muscle lengths/s. (L/s is a convenient measure of shortening velocity, as it is independent of the length of the muscle segment under consideration. Its dimension is s^{-1}, and not $L^{-1}\,s^{-1}$, as erroneously stated in the legend to figure 7 in He et al. (1999).) At the end of the shortening phase, the epifluorescence microscope head was lifted, and the fiber was transferred to relaxing solution and returned to its initial length. The fiber was then transferred to rigor solution, and the whole procedure was repeated up to three times with variations in the speed of the applied length change.

After the experiment the fiber was transferred to a test tube containing Laemmli (1970) solution for electrophoretic analysis.

The temperature of the microscope stage was adjusted to 12°C (or, alternatively, 20°C), and all subsequent steps and measurements were carried out at this temperature.

Data collection and analysis

Fluorescence, force, motor output, and sarcomere length signals were collected using a 12-bit analog-to-digital circuit operated at a minimum of 1 kHz (Computerscope; R. C. Electronics EGAA Computerscope, Goletta, CA; in an Intel Pentium 133 MHz computer). A chart recorder continuously monitored the force and fluorescence signal as a way of evaluating the state of the fibers. The fluorescence signal was converted into the amount of P_i released by the fibers as explained above.

In a typical record of tension three predominant phases were detectable: a first initial isometric phase, a shortening phase, and a final isometric phase (see Fig. 1, *A* and *B*). The ATP hydrolysis rate was determined from the slope of the fluorescence signal indicating P_i release: during the fixed-length (isometric) phases before and after the shortening phase, the slope was calculated over intervals of 0.15 mM P_i, which correspond to one hydrolytic cycle in all myosin heads, assuming a myosin active site concentration of 0.15 mM (Ferenczi et al., 1984). During the shortening phase the slope of the released P_i signal over time gave the ATP consumption rate related to active shortening at the preset shortening velocity.

The relatively constant tension level reached after photolytic release of ATP and before the applied length change was called isometric tension (P_o). During the shortening phase, tension declined, first steeply and then more slowly until the end of the shortening period: the average tension (P) during the slow decline period was considered as the tension during the shortening phase and expressed as a fraction of P_o to obtain the relative tension (P/P_o) utilized in the force-velocity relation. P multiplied by shortening velocity (V) was used to calculate mechanical power (W).

Relative force and shortening velocity pairs were interpolated with Hill's hyperbolic equation,

$$P/P_o = a \times (V_{max} - V)/(V + b) \quad (2)$$

where the fit parameters a, b, and V_{max} were obtained by least-square minimization.

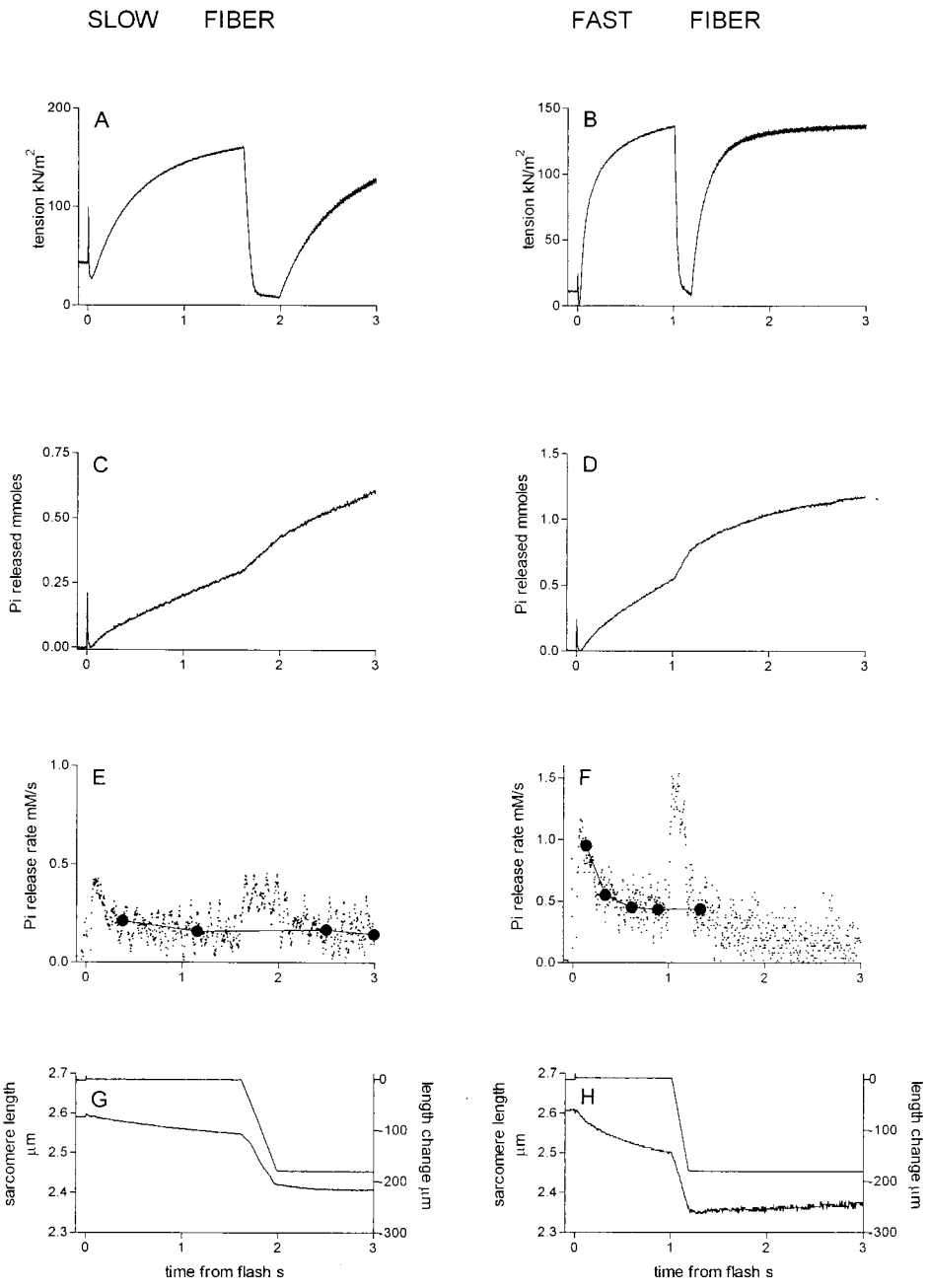

FIGURE 1 Typical experimental records of the contractions of a slow fiber segment (*left*) and of a fast fiber segment (*right*). (*A* and *B*) Tension records. The laser flash at time 0 resulted in the photolytic release of ATP. An initial fall in tension was followed by a tension rise. When tension nearly reached a plateau (and ATPase activity reached a quasi-steady state; see *C–F*) the fiber segment was allowed to shorten at a constant velocity (*G* and *H*), and tension decreased to a lower level. After the shortening period tension redeveloped, and a new plateau was reached. (*C* and *D*) Fluorescence signal, which, after calibration, provides a measure of P_i released by the hydrolysis of ATP. A fast initial phase was followed by a quasi-steady-state period. When the fiber was allowed to shorten, the gradient of the signal increased and, after the end of the shortening period, returned to the value before shortening. Saturation of the signal is seen (*D*) when total P_i released approached 1 mM. (*E* and *F*) The instantaneous derivative of the fluorescence signal corresponds to the rate of P_i release or ATP consumption. Note the fast initial phase, the quasi-steady state, the higher rate during the shortening phase, the return to the preshortening rate, and, in *F*, the decline due to saturation (after 1.5 s). The solid circles represent the average P_i release (or ATP hydrolysis) rate measured over intervals of 0.15 mM, which correspond to one complete hydrolytic cycle in all myosin heads (see Materials and Methods). (*G* and *H*) Motor output (*upper line*), i.e., the signal indicating the changes in the length of the fiber segment, and the sarcomere length signal (*lower line*). The sarcomere signal shows the internal shortening that takes place during the initial phases of contraction.

The same numerical values of the parameters were used in the power-velocity equation,

$$W = V \times a \times P_o \times (V_{max} - V)/(V + b) \quad (3)$$

The relation between ATP hydrolysis rate during active shortening (A_s) and shortening velocity was described by the following hyperbola (see He et al., 1999), where the numerical values of H, M, and D were obtained by least-square minimization:

$$A_s = H + M \times D \times V/(1 + D \times V) \quad (4)$$

The relation between A_s and relative load (P/P_o) was obtained by replacing V with its values expressed as a function of relative load (P/P_o) according to the force-velocity equation

$$V = b \times (1 - P/P_o)/(P/P_o + a) \quad (5)$$

Finally, the following equations describe the relations between efficiency (E) and shortening velocity (Eq. 6) and relative load (Eq. 7):

$$E = \frac{V \times a \times P_o \times (V_{max} - V)/(V + b)}{\Delta G_{ATP} \times (H + (M \times D \times V)/(1 + D \times V))} \quad (6)$$

$$E = \frac{P/P_o \times V \times P_o}{\Delta G_{ATP} \times (H + (M \times D \times V)/(1 + D \times V))} \quad (7)$$

where V is expressed as a function of P/P_o according to Eq. 5.

The free energy of ATP, ΔG_{ATP}, was assumed to be 50 kJ/mol (Kushmerick and Davies, 1969). The low concentration of P_i during ATPase measurements is likely to increase this value (this issue is addressed in the Discussion). The distance traveled by a myosin head during one hydrolytic cycle (D_{ATP}) (Irving and Woledge, 1981; Irving, 1991; Higuchi and Goldman, 1991) was determined from the ratio between sarcomere shortening velocity (V, expressed in nm/hs/s, hs = half-sarcomere) and ATPase rate during shortening (expressed in ATP/myosin head/s for a concentration of myosin heads of 0.15 mM). The number of attached myosin heads divided by the total number of myosin heads corresponds to the duty ratio (DR), the time fraction of the cycle each head spends in attached state. DR was calculated as the ratio of the working stroke distance (D_W) (assumed to be 10 nm) and D_{ATP}.

Data were expressed as the mean plus and minus one standard error, unless otherwise indicated. One-way variance analysis was used for comparison between fiber groups. The least-square minimizations were carried out with the analysis software Prism (GraphPad). Richardson's method was used to evaluate the partial derivatives of the cost function with respect to each parameter.

Model analysis

The results were simulated using a kinetic scheme of the ATPase cycle (Scheme 1) representing the predominant flux. The ATPase rate was calculated from the rate of P_i release according to a set of differential equations describing the enzymatic reaction pathway. The scheme was based on four attached and two detached states, the six transitions between the states being approximated by the mass action law. The numerical values of the forward and reverse rate constants, k_i and k_{-i}, for the ith step were defined as described in the legends to Figs. 9 and 10. The parameters k_3 and k_6 were allowed to vary to fit the model predictions to the experimental results (force-velocity curves). The force developed, in arbitrary units, was calculated according to the relation

$$\text{Force} = c \times ([\text{A·M·ADP·P}_\text{i}] + [\text{A·M·ADP}] + 0.1 \times [\text{A·M}])$$

where c is a proportionality constant, and it is assumed that rigor cross-bridges produce only 10% of the force produced by active attached cross-bridges (A·M·ADP·P_i and A·M·ADP), thus accounting for the nonzero force before photolytic release of ATP.

$$\begin{array}{ccccc} \text{A·M·} + \text{ATP} & \overset{1}{\rightleftarrows} & \text{A·M·ATP} & \quad \text{A·M·ADPP} \overset{5}{\rightleftarrows} \text{A·M·ADP} \overset{6}{\rightleftarrows} \text{A·M} \\ & & 2\uparrow\downarrow & \quad 4\uparrow\downarrow & \\ & & \text{M·ATP} \overset{3}{\rightleftarrows} \text{M·ADPP} & & \end{array}$$

SCHEME 1 The six-step reaction pathway for the actomyosin, ATPase in muscle fibers, as used in the simulations.

Calculations were carried out with a Euler-stepping algorithm with time intervals of 0.01 μs. The program was written in Fortran and was compiled and run on an Intel Pentium II personal computer. Increasing the time interval to 0.1 μs had no effect on the simulated curves.

RESULTS

Fiber identification and grouping

Mechanical and energetic parameters were determined in 55 fibers. On the basis of the electrophoretical separation of MHC isoforms, the fibers were classified into one of four groups: slow or type 1, which contained only MHC-1 (also called β/slow); type 1–2A, which contained MHC slow and MHC-2A; type 2A, which contained only MHC-2A; and type 2A-2B, which contained both fast isoforms MHC-2A and MHC-2X. (Note that the traditional fiber nomenclature is used, despite the identification of the MHC isoform contained in the 2B fiber as MHC-2X (see Smerdu et al., 1994).) No pure 2B fibers, i.e., fibers containing only MHC-2X, were found. Average (± SE) cross-sectional areas and lengths of the active segments were as follows: type 1: 6135 ± 452 μm^2 and 2.51 ± 0.06 mm (n = 29); type 1–2A: 8878 ± 1548 μm^2 and 2.25 ± 0.19 mm (n = 4); type 2A: 8611 ± 876 μm^2 and 2.39 ± 0.11 mm (n = 17); type 2A-2B: 5350 ± 418 μm^2 and 1.97 ± 0.08 mm (n = 5).

ATP consumption rate during isometric contraction and at rest

Fig. 1 shows typical experimental records of force development, shortening, and P_i liberation in a slow and a fast human muscle fiber at 12°C. After the photolytic release of ATP, active tension developed and ATP hydrolysis led to the release of P_i, which was detected as an increase in the fluorescence signal. The rate of tension rise was greater in fast (Fig. 1 *B*) than in slow (Fig. 1 *A*) fibers. Moreover, the gradient of fluorescence signal (compare Fig. 1, *C* and *D*; note the different scales) and the amplitude of its derivative (see Fig. 1, *E* and *F*) were greater in fast (*right*) than in slow (*left*) fibers. When the fiber was allowed to shorten, tension decreased and the P_i release rate quickly increased, as indicated by the higher gradient of the fluorescence signal. At the end of the shortening phase, tension redeveloped and the P_i release rate returned to the value before shortening.

The ATP consumption rate during the initial isometric contraction declined after an initial transient fast phase to a quasi-steady-state value. The decline was more pronounced in fast fibers than in slow fibers. In fast fibers the quasi-steady-state condition was reached after 0.6–0.8 s, or four ATP turnovers (assuming a myosin head concentration of 0.15 mM; see Materials and Methods), with an ATPase rate that was ~50% of the initial ATPase rate. In slow fibers a quasi-steady-state condition was also reached after 0.6–0.8 s, corresponding in this case to the completion of the first ATP turnover with an ATPase rate that was 80% of the initial value.

Mean values of peak isometric tension, ATP hydrolysis rate at the third turnover, and tension cost (ratio between ATP consumption rate at the third turnover and peak tension) in the four groups of fibers with distinct MHC isoform composition are shown in Fig. 2. The statistical comparison shows large and significant differences in ATP consumption rate and tension cost, whereas isometric tension values were not significantly different.

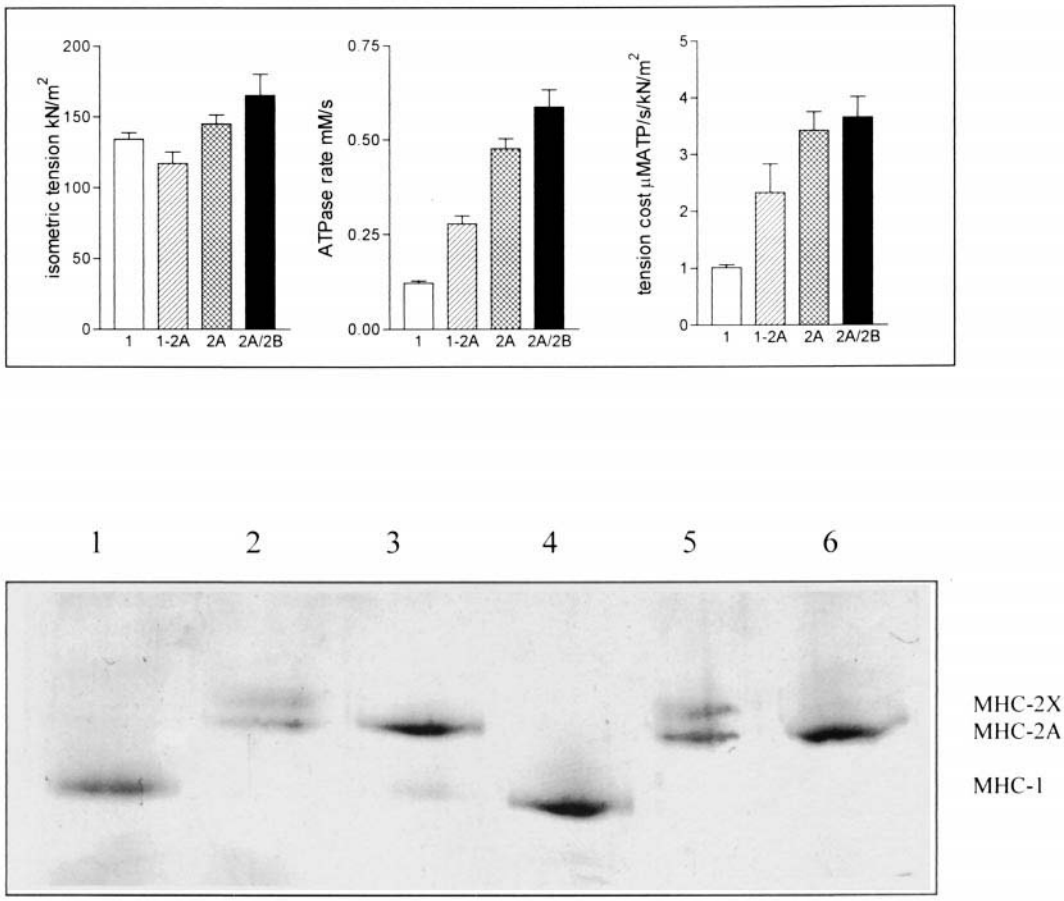

FIGURE 2 Functional and molecular characterization of the fiber groups. (*Top*) Mechanical and energetic parameters of the isometric contraction. The histograms show the average values of isometric tension, ATPase activity, and tension cost during the third ATP turnover in isometric contractions of the four groups of fibers at 12°C. The third ATP turnover corresponds to ~0.6–0.8 s after the beginning of the contraction in fast fibers and to 2–3 s in slow fibers. Variance analysis indicates no significant differences in isometric tension, significant differences in ATPase activity between all groups, and significant differences in tension cost between all groups, except between 2A and 2A/2B. (*Bottom*) A typical electrophoretic separation of MHC isoforms in six single fibers: slow fibers (containing MHC-1) in *lanes 1* and *4*, fast 2A fibers in *lanes 3* and *6*, fast 2A/2B fibers (containing both MHC-2A and MHC-2X) in *lanes 2* and *5*.

The ATP consumption rate at rest was determined in four slow fibers and in four fast 2A fibers. The average (± SE) values (5.1 ± 0.65 and 3.5 ± 0.45 μM/s in slow and fast fibers, respectively) were not significantly different. ATP consumption at rest was ~1% of the values reached during isometric contractions and ~500 times slower than the ATPase rate during shortening at the highest velocity.

Force-velocity properties

Velocity and average force were measured during periods of imposed fiber shortening at a constant velocity (isovelocity releases) during maximum calcium activation of the fibers. Hyperbolic Hill equations (Eq. 2) were fitted to the data for three fiber groups (slow, fast 2A, and fast 2A-2B) as described in Materials and Methods. Too few data points for type 1–2A were available to obtain a reliable fit. The numerical values of the parameters are reported in Table 1. Force-velocity and power-velocity data points together with the best fit of the Hill's hyperbolic equations and the power-velocity curves are shown in Fig. 3 for slow and fast 2A fibers.

Each fiber type exhibited distinct values of maximum shortening velocity (V_{max}), peak power (W_{max}), and optimal velocity (V_{opt}, velocity at which peak power is produced). As expected (Bottinelli et al., 1996), the values of maximum shortening velocity and peak power were higher in fast 2A fibers (0.88 L/s and 7.3 W/l for V_{max} and W_{max}, respectively) than in slow type 1 fibers (0.37 L/s and 1.9 W/l). Fast 2A-2B fibers reached still higher values of maximum shortening velocity and peak power (1.01 L/s and 9.5 W/l). Variance analysis showed that the differences between fast 2A and slow fibers were statistically significant, whereas the difference between type 2A and type 2A-2B did not reach statistical significance. Optimal velocity was about

TABLE 1 Parameters of the force-velocity equations and of the ATP hydrolysis rate-velocity equations for the different fiber groups at 12°C and 20°C

	12°C			20°C	
Fiber type	1	2A	2A-2B	1	2A
Parameters of the force-velocity Hill equation (Eq. 2)					
a (P_o fraction)	0.07 ± 0.02	0.13 ± 0.06	0.15 ± 0.04	0.07 ± 0.04	0.14 ± 0.03
b (L/s)	0.03 ± 0.02	0.12 ± 0.06*	0.17 ± 0.02	0.08 ± 0.01	0.30 ± 0.03
V_{max} (L/s)	0.37 ± 0.06	0.88 ± 0.12*	1.01 ± 0.14*	1.15 ± 0.36‡	2.37 ± 0.34‡
P_o* (P_o fraction)	0.78	0.92	0.92	1.01	1.28
Parameters of the relation between ATP hydrolysis rate and velocity (Eq. 4)					
H (mM/s)	0.13 ± 0.02	0.43 ± 0.06*	0.55 ± 0.04*†	0.22 ± 0.09	0.78 ± 0.31
M (mM/s)	6.70 ± 3.0	5.54 ± 1.27	50.8 ± 4.8*†	0.79 ± 0.48	1.70 ± 1.16
D $(L/s)^{-1}$	0.12 ± 1.53	0.29 ± 0.09	0.03 ± 0.01	2.79 ± 3.90	1.43 ± 2.50
$1/D$ (L/s)	8.4	3.44	32.2	0.35	0.70

Numerical values of the parameters are given with their standard errors. The results of statistical comparison between numerical values of the parameters obtained in different fiber types are also shown: *significant difference from type 1; †significant difference from type 2A; ‡significant difference from the same fiber type at 12°C. $P_o^* = V_{max} \times a/b$.

three times higher in fast (0.23 L/s in 2A fibers and 0.28 L/s in 2A-2B fibers) than in slow (0.083 L/s) fibers. The ratio between optimal velocity and V_{max} was 0.22 for slow fibers, 0.26 for 2A fibers, and 0.28 for 2A-2B fibers.

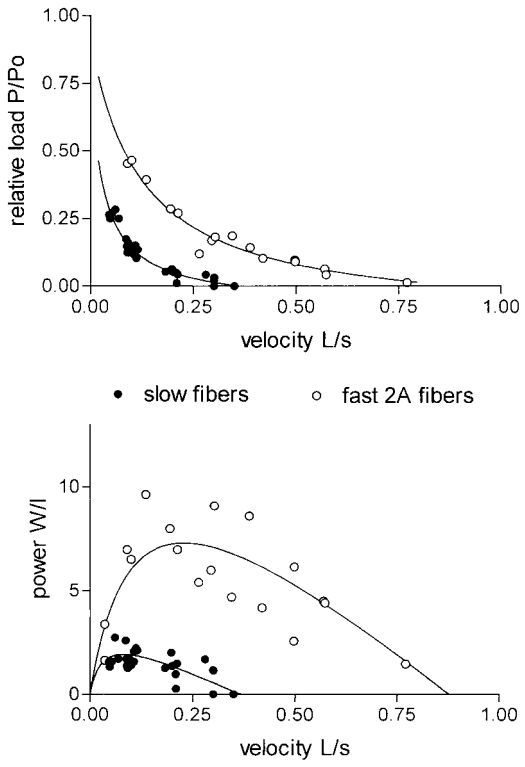

FIGURE 3 Force-velocity and power-velocity curves. (*Top*) Force-velocity data obtained in slow (●) and fast (○) 2A fibers at 12°C. Data are interpolated with Eq. 2, the parameters of which are reported in Table 1. (*Bottom*) Power-velocity curves of slow and fast 2A fibers at 12°C. The power-velocity data points are interpolated (Eq. 3), using the same parameters obtained from fitting force-velocity curves. Note the diversity in maximum shortening velocity, in peak power, and in the velocity at which peak power is reached (optimal velocity).

Sarcomere length changes

The sarcomere length signal was recorded in 32 of the 55 fibers. Despite the measures taken to reduce compliance of the damaged ends and therefore the "internal" shortening, a significant movement occurred during initial tension development in virtually all fiber segments (see Fig. 1). During the first second after photoliberation of ATP, total sarcomere shortening was on average 1.44 ± 0.19% L (n = 20, ± SE) in slow fibers and 3.04 ± 0.40% L (n = 12) in fast 2A fibers. This corresponded to an average initial speed of sarcomere shortening (calculated in the first 200 ms after the flash) of 0.045 L/s for fast fibers and 0.011 L/s for slow fibers.

The sarcomere shortening velocity was also calculated during the isovelocity release, in 18 fibers in which the diffraction pattern did not deteriorate during shortening (see Materials and Methods). Once expressed in L/s, sarcomere shortening velocity was compared with the shortening velocity imposed on the fiber segments. Regression analysis showed that sarcomere shortening velocity and segment shortening velocity were highly correlated: the slope was 0.963 ± 0.023 ($p < 0.001$) and was not significantly different from 1. This indicates a full correspondence between measurements of sarcomere and of segment shortening velocity during applied shortening.

ATP consumption during active shortening

During isovelocity shortening the ATP consumption rate increased above the isometric level (A_o) and reached a new steady value (A_s) (Fig. 1). The ATP consumption rate during shortening (A_s) was roughly proportional to shortening velocity. The relations between A_s and velocity were interpolated with hyperbolic equations (Eq. 4). The parameters obtained by least-square minimization are reported in Table 1. As can be seen in Fig. 4 A, virtually no plateau and no

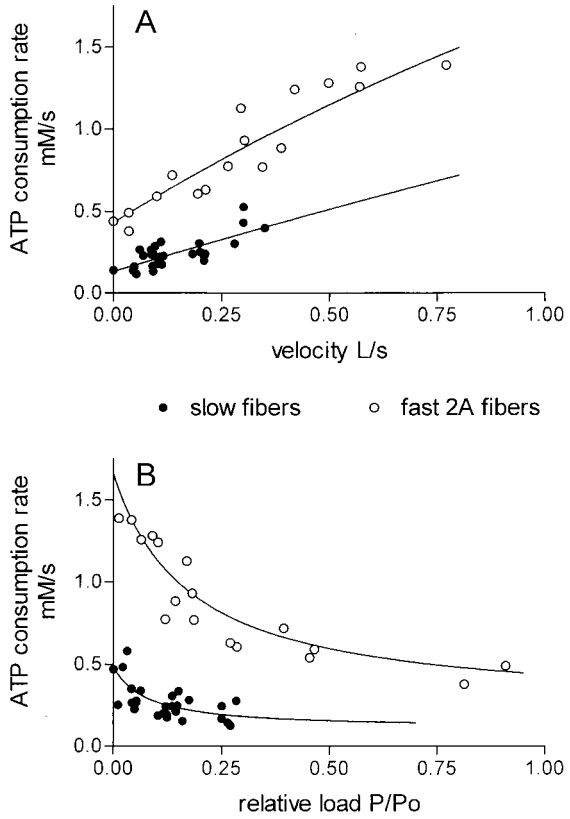

FIGURE 4 ATP consumption rate during isovelocity shortening at 12°C. (*A*) Relation between ATP consumption rate during shortening (A_s) and shortening velocity in slow (●) and fast 2A (○) fibers. Hyperbolic fits (Eq. 4) to the data are shown (*continuous lines*, fit parameters given in Table 1). (*B*) Relation between A_s and relative load (P/P_o). The curves (obtained from Eq. 4, replacing V according to Eq. 5) are drawn using the parameters obtained by fitting the force-velocity curves (Eq. 2; see Fig. 3) and A_s-velocity curves (*A* in this figure).

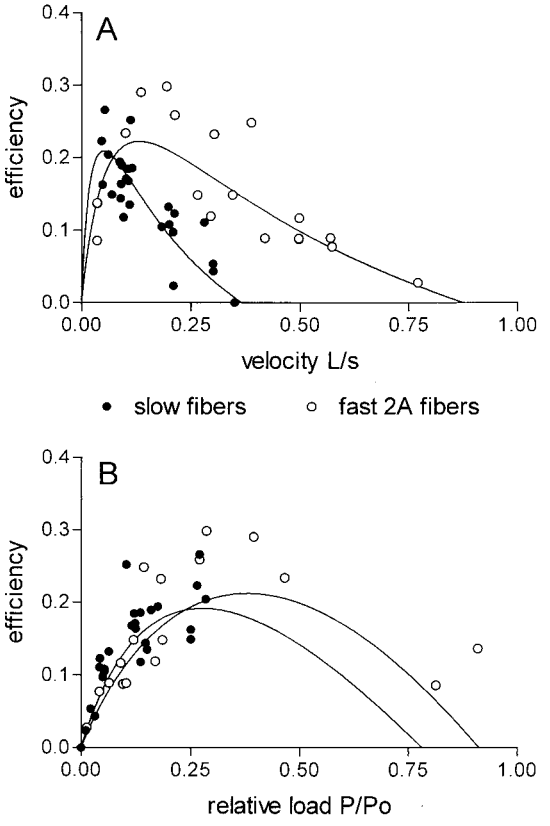

FIGURE 5 Thermodynamic efficiency in relation to shortening velocity and load at 12°C. The values of efficiency (calculated as the ratio of mechanical power over the rate of energy release) are plotted versus shortening velocity (*A*) and relative load (*B*) for slow and fast 2A fibers. Data are interpolated by curves (Eqs. 6 and 7) obtained with the numerical values of the parameters calculated by fitting the force-velocity curves and the curves of the ATP consumption rate versus shortening velocity.

decrease were detectable, even at speeds close to maximum shortening velocity. This is confirmed by the hyperbolic fitting, as the high values of the asymptote ($H + D \times M$) and of the velocity ($1/D$) at which half of the asymptotic value is reached indicate that the ranges of velocity explored are in the initial quasilinear region of the curve. In Fig. 4 *B*, the rate of ATP consumption is expressed as a function of the relative load, and an inverse correlation between ATP consumption rate and load is visible.

Efficiency

Thermodynamic efficiency was calculated by dividing mechanical power by the rate of energy release in slow fibers (type 1), in fast 2A and in fast 2A-2B fibers. The rate of energy release was obtained as the product of ATP consumption rate and the free energy of ATP hydrolysis (50 kJ/mol; see Materials and Methods and Discussion). In Fig. 5 the values of efficiency are plotted versus shortening velocity or versus relative load for slow and fast 2A fibers. The data points are interpolated using Eq. 6 (Fig. 5 *A*) and 7 (Fig. 5 *B*; see Materials and Methods) with the parameter values reported in Table 1.

Peak efficiencies ranged between 0.21 (slow fibers) and 0.27 (fast 2A-2B fibers) and were similar in all fiber types; the differences were not statistically significant. On the other hand, peak efficiencies were reached at higher ($p < 0.01$) speed of shortening (0.15 L/s) and greater ($p < 0.05$) relative load (0.36 P/P_o) in fast 2A fibers compared to slow fibers (0.05 L/s and 0.27 P/P_o, respectively). Interestingly, in all fiber groups peak efficiency was reached at a shortening velocity lower than optimal velocity for mechanical power.

Temperature sensitivity of ATP consumption rate and efficiency

In a subset of 10 slow and seven fast 2A fibers the mechanical power, the rate of ATP consumption, and the efficiency

were determined at 20°C. In some fibers the measurements were repeated at both 12°C and 20°C.

Force-velocity and power-velocity curves at 12°C and 20°C are shown in Fig. 6. The values of the parameters of the force-velocity curves are reported in Table 1. As expected, the temperature increase caused a marked rise in maximum shortening velocity (2.7–2.9 times) and in peak power (3.8 times). The ratio between optimal velocity and V_{max} remained virtually unchanged: 0.21 in slow fibers and 0.25 in fast 2A fibers. The Q_{10} values of V_{max} were 3.85 and 3.46 for slow and fast fibers, respectively, whereas the Q_{10} values of peak power were 5.35 and 5.41 for slow and fast fibers. Isometric tension (P_o) increased by ~20%, reaching, at 20°C, 150 ± 8 kN/m^2 (n = 10, ± SE) in slow fibers and 170 ± 15 kN/m^2 in fast 2A fibers (n = 7).

The ATPase rates during isometric contraction also increased with temperature: the values measured during the third ATP turnover (see above) reached 0.24 mM/s for slow fibers and 0.65 mM/s for fast 2A fibers. This corresponds to Q_{10} values of 2.2 and 2.09, respectively. ATPase rates measured during shortening (A_s) at velocities up to ~60% V_{max} increased in proportion to shortening velocity (see Fig. 7, *A* and *B*); at each velocity the ATP consumption rate was higher in fast than in slow fibers. The relations between A_s and shortening velocity were interpolated with hyperbolic curves (Eq. 4), the parameters of which are reported in Table 1. As shown in Fig. 7, *A* and *B*, a trend toward a plateau of A_s is visible in both slow and fast fibers at 20°C. The enhanced curvature of the relation between A_s and shortening velocity is confirmed by the reduction of the velocity ($1/D$) at which half of the asymptotic value is reached (see Table 1). Efficiency was then derived as the ratio between mechanical power output and the rate of energy release. As the temperature-dependent increase in power output was greater than the increase in ATPase rate, peak efficiency showed a pronounced increase (see Fig. 7, *C* and *D*). Peak efficiency at 20°C reached 0.34 in slow fibers and 0.41 in fast fibers; the difference between fiber types was not statistically significant.

Actin-myosin interaction kinetics in slow and fast 2A fibers

The distance traveled by a myosin head during one hydrolytic cycle (D_{ATP}) was determined for slow and fast 2A fibers from the ATPase rate during shortening (A_s, expressed in ATP/myosin head/s for a concentration of myosin heads of 0.150 mM) and sarcomere shortening velocity (V, expressed in nm/hs/s), as described in Materials and Methods. D_{ATP} increased with the velocity of shortening and at each velocity was longer in type 1 fibers than in type 2A fibers (see Fig. 8 *A*). This follows from the lower ATPase rate of type 1 fibers when compared to type 2A fibers (Fig. 4 *A*). In both fiber groups, because of the higher ATPase at 20°C than at 12°C, the distance traveled in one hydrolytic cycle was reduced by increasing temperature.

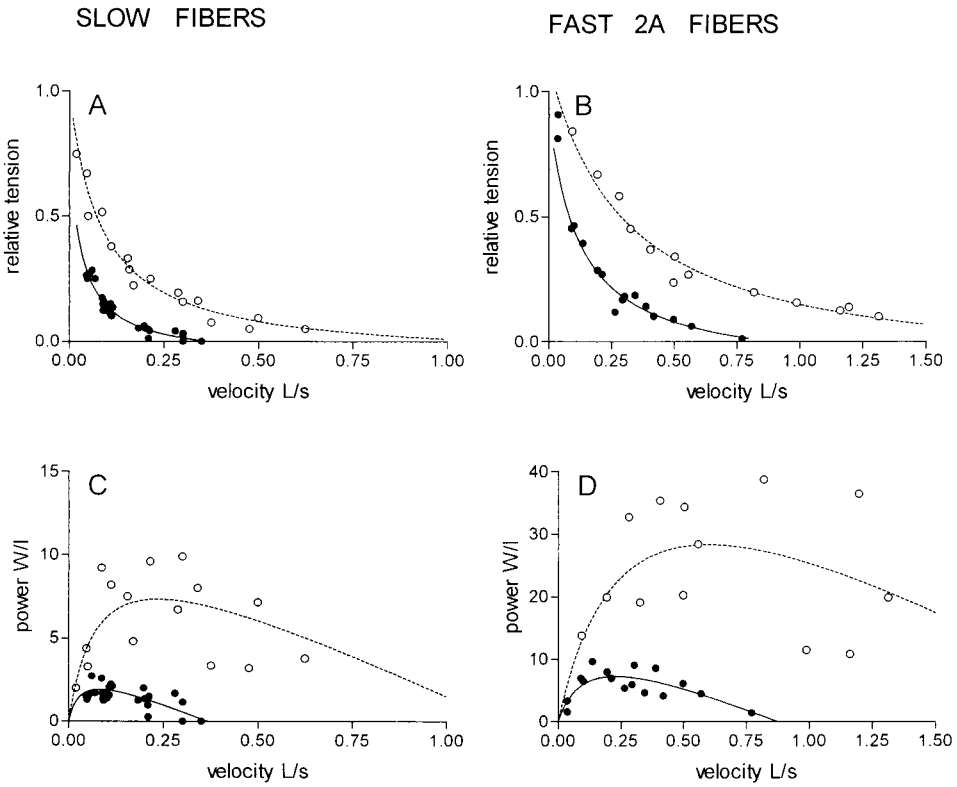

FIGURE 6 Effect of temperature on force-velocity and power-velocity curves. Force-velocity curves of slow (*A*) and fast 2A (*B*) fibers at 12°C (*filled circles and continuous lines*) and 20°C (*empty circles and dashed lines*) and power-velocity curves for the same slow (*C*) and fast (*D*) fibers at 12°C and 20°C (same symbols as in *A* and *B*). The parameters of the force-velocity (Eq. 2) and power-velocity (Eq. 3) curves are listed in Table 1.

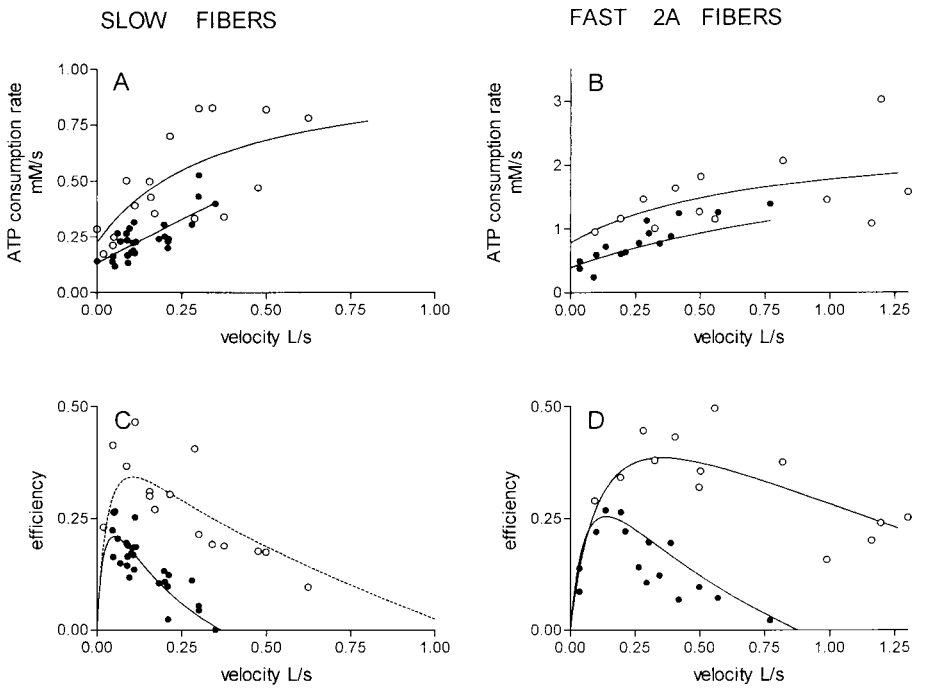

FIGURE 7 Effect of temperature on the rate of ATP consumption and on thermodynamic efficiency. (*A* and *B*) Relation between the rate of ATP consumption during shortening (A_s) and shortening velocity in slow fibers (*A*) and fast 2A fibers (*B*) at 12°C (●) and 20°C (○). The parameters of the hyperbolas fitted to the data points are reported in Table 1. (*C* and *D*) Relation between efficiency and shortening velocity in slow fibers (*C*) and fast 2A fibers (*D*) at 12°C and 20°C (same symbols as in *A* and *B*). The parameters of the curves (Eq. 6) that interpolate the experimental data are reported in Table 1.

The duty ratio (DR), i.e., the fraction of myosin heads attached to actin or the fraction of time each myosin head spends in attached state, was calculated for both slow and fast 2A fibers as the ratio between the working stroke distance (D_W) and the distance traveled per hydrolytic cycle (D_{ATP}). On the basis of existing evidence derived from single-molecule studies (Lauzon et al., 1998; Sugiura et al., 1998), it was assumed that D_W is equal in slow and fast myosins and corresponds to 10 nm (see Discussion). As shown in Fig. 8 *B*, DR decreased with increasing velocity and, at each velocity, was higher for type 2A than for type 1 fibers. For both fiber types, DR was higher at 20°C than

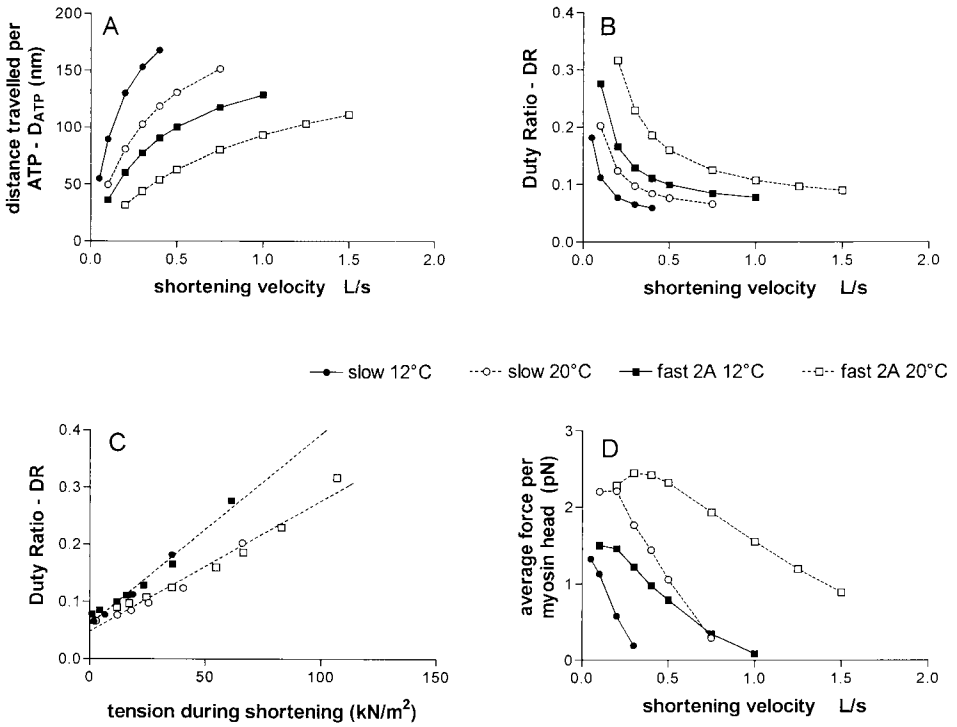

FIGURE 8 Parameters of the actin-myosin interaction inferred from shortening velocity, tension development, and ATP hydrolysis rate. (*A*) Distance traveled per ATP hydrolyzed (D_{ATP}), plotted versus shortening velocity in slow and fast 2A fibers at 12° and 20°C. (*B*) Duty ratio (DR) plotted versus shortening velocity, in slow and fast 2A fibers at 12° and 20°C. (*C*) Duty ratio plotted versus active tension in slow and fast 2A fibers at 12° and 20°C. (*D*) Average force per attached cross-bridge at various shortening velocities in slow and fast 2A fibers at 12° and 20°C.

at 12°C. In Fig. 8 *C*, DR is plotted versus tension during shortening for type 1 and type 2A fibers at 12°C and 20°C. At each temperature, the linear regressions to data points from type 1 and type 2A fibers virtually superimposed. For the sake of clarity, data points from type 1 and type 2A fibers at each temperature were pooled together and fitted by a single linear regression. As expected, the lower the tension (i.e., the higher the velocity), the lower the DR. Interestingly, with increasing velocity of shortening (Fig. 8 *B*) or reduced load (Fig. 8 *C*), DR tended to approach a lower limit, DR at V_{max} (zero tension), which was the same for type 1 and type 2A fibers and very similar at 12°C and at 20°C (0.06 and 0.07, respectively). The fact that, at each tension, type 1 and type 2A fibers had the same DR indicates that the force developed by a myosin head was the same. It should be pointed out, however, that at each tension type 2A fibers shortened at a much higher velocity than type 1 fibers.

At 20°C, for both type 1 and type 2A fibers, force was developed with a lower fraction of attached bridges than at 12°C. This indicates that an increase in force per myosin head contributes to the well-known increase in force that follows an increase in temperature. This effect was virtually identical for slow and fast 2A myosins. The average force per attached myosin head was calculated, as proposed by Linari et al. (1998), from DR, developed tension, and density of myosin heads per cross-sectional area (0.5×10^{15} thick filaments/m^2, 290 myosin heads/filament; Linari et al. 1998). As can be seen in Fig. 8 *D*, where the average force per attached myosin head is plotted versus shortening velocity, at each speed, average forces were higher in fast than in slow fibers, and ~1.5 times higher at 20°C than at 12°C in both fiber types.

DISCUSSION

Mechanical power, ATP consumption rate during shortening, and thermodynamic efficiency of single muscle fibers isolated from human muscles were measured to compare chemomechanical transduction in slow and fast 2A sarcomeric myosin isoforms. The results obtained showed that during active shortening the ATP consumption rate increased in proportion to shortening velocity and in proportion to the consumption rate in isometric contraction before the shortening phase. Thus, fast myosins, which consumed more energy in isometric conditions, were also more expensive during shortening. Peak efficiency, however, was not significantly different in fast and slow fibers, although it was reached in the former at a velocity that was three times higher. An increase in temperature from 12° to 20°C caused a marked increase in mechanical power, ATP consumption rate, and efficiency for all fiber types.

The results can be simulated by the kinetic scheme of the ATPase cycle (Scheme 1), with the three following assumptions: 1) that the forward rate constant k_6 of the ADP release step, which is the rate-limiting step for actin-myosin detachment, depends on the load on the muscle, so that at low loads, k_6 is accelerated; 2) that the hydrolysis step rate constant k_3, which limits the rate of attachment of myosin to actin, is faster in fast than in slow fibers; and 3) that the force is proportional to the concentration of attached myosin heads, with AM·ADP·Pi and AM·ADP producing the same force and AM producing 10% of that produced by AM·ADP. An example of such a simulation for a slow fiber at 12°C is shown in Fig. 9. The assumptions for the effect of load on k_6 and accounting for the difference in fiber types with a difference in k_3 result in a good fit to the force-velocity curves (Fig. 10 *A*) and allow simulation of the Fenn effect, namely an increase in ATP consumption with shortening velocity (Fig. 10 *B*).

Comparison with previous results

The results are in broad agreement with previous results on single muscle fibers of humans (Bottinelli et al., 1996; Stienen et al., 1996; Larsson and Moss, 1993; Widrick et al., 1996) and of other species, where large differences in maximum shortening velocity (V_{max}), peak power (W_{max}), optimal velocity (V_{opt}), isometric ATPase activity (A_o), and tension cost were found between slow (type 1) and fast (2A and 2A-2B) fibers. On the other hand, isometric tension (P_o) was similar across all fiber groups.

Whereas the values of V_{max} and V_{opt} were comparable to those obtained previously (Bottinelli et al., 1996; Stienen et al., 1996) at the same temperature (12°C), the values of P_o and A_o were greater. This might be attributed to a possible effect of low P_i concentration produced in the present experimental condition by the P_i mop (MEG-PNPase) and MDCC-PBP. Isometric tension developed by fast fibers in the present experimental conditions (i.e., with micromolar P_i concentrations (145–165 kN/m^2)) was ~25% higher than that measured in previous experiments (107–132 kN/m^2; Stienen et al., 1996), where the P_i concentration was expected to be 0.5 mM (Potma et al., 1995; Potma and Stienen, 1996). The increase in force by a factor of 20–27% achieved by reducing P_i is in accordance with the prediction of the isometric tension-P_i relation calculated at very low P_i concentrations for rabbit fast psoas fibers by Pate et al. (1998). The effect of reducing P_i was twofold higher in slow fibers. This might be explained either by a higher sensitivity of slow fibers to P_i concentration, in partial agreement with the results of Potma et al. (1995) and Wang and Kawai (1997), or by specific sensitivity of slow fibers to ADP (Horiuti et al., 1997). Although the presence of the ADP-regenerating system (creatine kinase/phosphocreatine) in the solution reduces the variation in ADP concentration in the fibers during the experiments, it may not completely eliminate a transient increase in ADP concentration during periods of highest ATP utilization. In the experiments of Stienen et al. (1996), in which the NADH-enzyme system

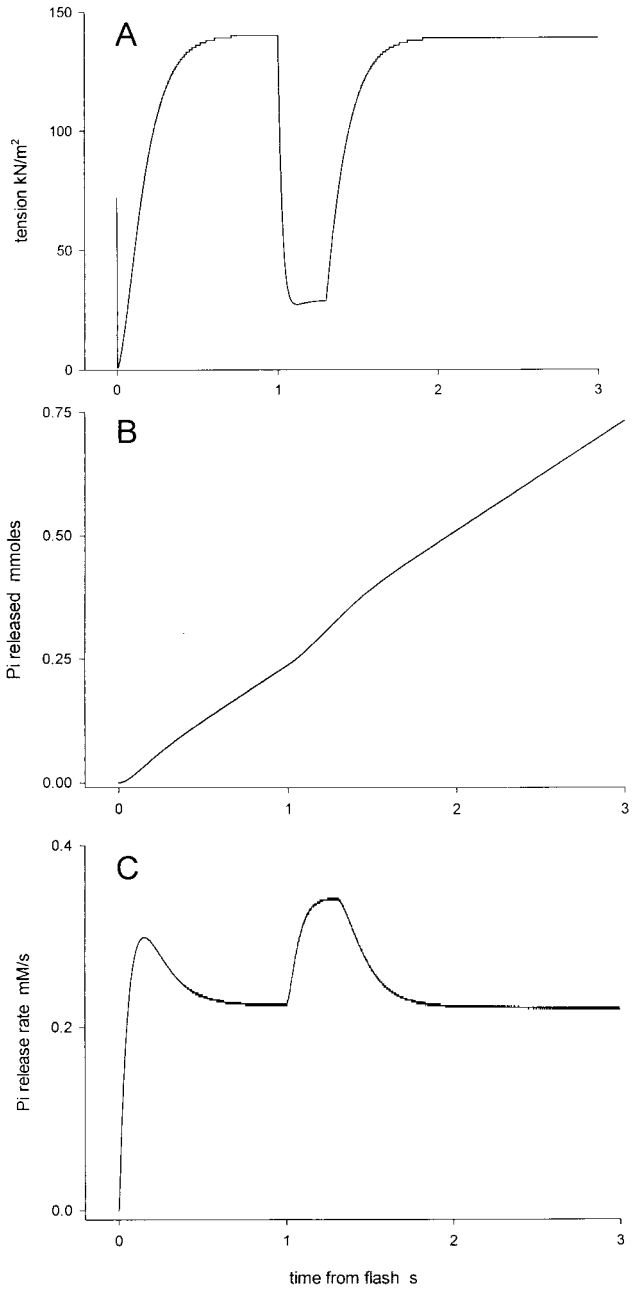

FIGURE 9 Simulation of the ATPase kinetic scheme for a slow fiber at 12°C as obtained experimentally in Fig. 1, *A*, *C*, and *E*. Values for the rate constants were $k_1 = k_2 = 1 \times 10^6\ M^{-1}s^{-1}$; $k_{-1} = 10\ s^{-1}$; $k_2 = k_4 = 1 \times 10^5\ M^{-1}\ s^{-1}$; $k_3 = 3\ s^{-1}$ (for fast fibers, $k_3 = 10\ s^{-1}$); $k_5 = 100\ s^{-1}$; $k_{-5} = k_{-6} = 1000\ M^{-1}\ s^{-1}$; $k_6 = 4\ s^{-1}$. The time interval used in the calculations was 1×10^{-7} s. A. At time 0, the ATP concentration increased instantaneously from 0 to 1.5 mM, causing rigor force to drop, and soon thereafter active force to develop, as calculated by force $= c \times$ ([A·M·ADP] + [A·M·ADP·P_i] + 0.1 × [A·M]), where $c = 2.39 \times 10^6$. At 1 s, shortening is simulated by increasing the value of k_6 from 4 to 10 s^{-1}. Force is seen to drop quickly to 20% of the value before shortening. (*B*) Simulation of P_i released during the protocol. (*C*) Derivative of trace *B*, giving the rate of P_i release. Acceleration of the ATPase during shortening is clearly seen, as is the high ATPase rate immediately following the photolytic release of ATP

was used to monitor ATP utilization, a gradient of ADP and ATP concentrations may have established itself across the thickness of the fibers, as discussed by He et al. (1997). Interestingly, the ATP consumption rate (A_o) in isometric conditions was also higher than previously determined. Potma et al. (1995) showed that in slow but not in fast fibers of the rabbit, isometric tension and isometric ATPase were equally sensitive to changes in P_i concentration. The comparison of the values of A_o obtained in this study with values previously obtained (Stienen et al., 1996) suggests that in both fast and slow human fibers A_o and P_o vary with P_i concentration in a similar way. As a consequence, tension cost remains rather constant over a large range of P_i concentration.

The effects of temperature on the force-velocity relationship and on ATP consumption in isometric contraction were similar to those previously observed in human fibers (Bottinelli et al., 1996; Stienen et al., 1996). In particular, in the range of temperature examined (12–20°C), V_{max} and W_{max} showed a much higher thermal sensitivity than A_o, and the effect of temperature on P_o was much lower.

Previous measurement of the rate of P_i release during maximum calcium activation in rabbit fast (psoas) and slow (soleus) fibers with the high time resolution provided by the fluorescent MDCC-PBP assay revealed a very high initial P_i release rate followed by a decline (He et al., 1997, 1998a,b, 1999). In most cases MDCC-PBP saturated before a steady state in ATP consumption rate was reached. Fast and slow human fibers examined in this study also showed an initially high ATPase rate. However, because of the lower ATPase rate in human muscle fibers compared to rabbit fibers, a phase of steady ATPase activity was reached during the isometric phase of contraction before saturation of the probe, particularly in slow fibers.

Compared to the quasi-steady-state condition, the initial fast rate was 50% greater in fast fibers and only 20% greater in slow fibers. A part of this initial high ATPase activity is due to internal shortening. From the speeds of internal (sarcomere) shortening during the initial phase and the relation between ATP consumption and shortening velocity, it can be calculated that during the initial phase of contraction shortening accounts on average for increases in ATPase activity of 6% and 11% in slow and fast fibers, respectively. The model simulation (Fig. 9) also shows a high initial ATPase, which is a direct consequence of the kinetic scheme and is a phenomenon distinct from any increase in ATPase due to initial shortening. The initial high rate of P_i release occurs because with the given values of the rate constants, AM·ADP accumulates at the expense of A·M·ADP·P_i until the quasi-steady state is reached. This is accompanied by a transient rate of P_i release in excess of the steady-state ATPase during the isometric state. The amplitude of the transient P_i release is necessarily less than one turnover (0.15 mM), as found experimentally (data not shown).

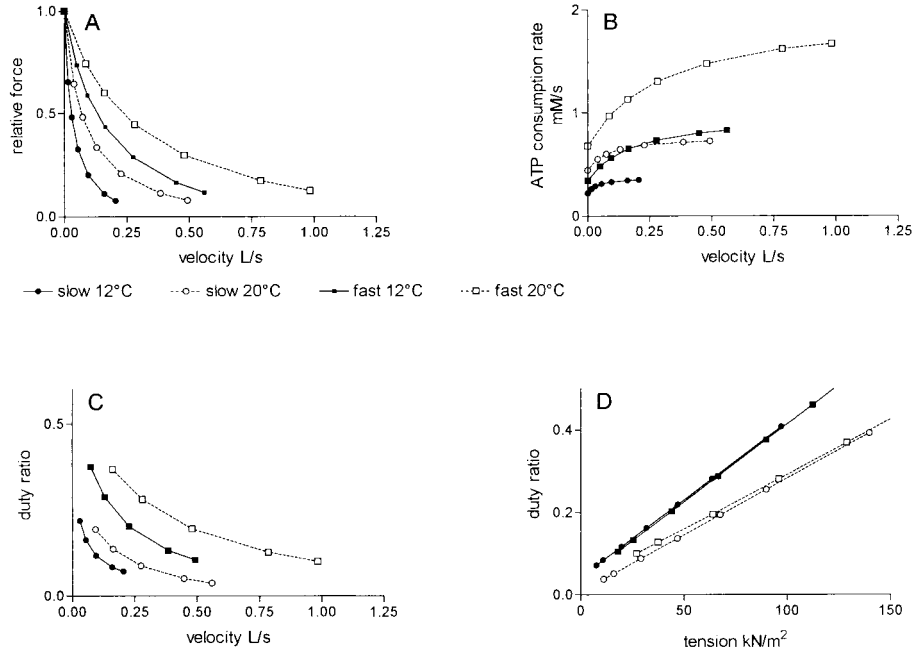

FIGURE 10 A series of simulations of Scheme 1 such as that shown in Fig. 9 were used to compile the model predictions shown here. The symbols represent the same fiber types as in Fig. 8 and the values calculated from the model. These are joined by straight line segments. (*A*) Force-velocity curves of slow and fast 2A fibers at 12°C and 20°C. k_6 was varied over the range 4–400 s^{-1} to simulate load sensitivity of the rate constant controlling ADP release, and the corresponding shortening velocity was calculated from the force-velocity relation, using the parameters shown in Table 1. The differences between fast and slow fibers resides in a difference in the hydrolysis step k_3. For simulations of fiber characteristics at 20°C, all rate constants were increased by a factor of 2 compared to the values for 12°C, and the force per attached cross-bridge was assumed to be 1.5 times that at 12°C. (*B*) Simulation of ATP consumption rate during shortening (cf. Fig. 8, *A* and *B*). (*C*) Duty ratio versus shortening velocity (cf. Fig. 9 *B*). (*D*) Duty ratio versus tension (cf. Fig. 8 *C*).

Fenn effect

Because of its high sensitivity and time resolution, the MDCC-PBP assay is suited to the study of the increase in ATP consumption during shortening, an effect known as the Fenn effect (Goldman, 1987; Potma et al., 1994). The results obtained in this study consistently show an increase in the ATP consumption rate during active shortening in both slow and fast fibers. The ATP consumption rate increased in direct relation to shortening velocity. At low temperature (12°C) no plateau and no decrease were detectable, even at speeds close to maximum shortening velocity. This is in contrast with several previous reports (Barclay et al., 1993; Linari and Woledge, 1995). In contrast, at 20°C a trend toward a plateau in the rate of energy release was visible in both slow and fast fibers (see Fig. 7, *A* and *B*).

As shown in Figs. 9 and 10 *B*, the model predicts the increase in ATP hydrolysis during shortening. In Fig. 9 the rate of P_i release is seen to increase rapidly with the addition of ATP. Then P_i release reaches a steady state during the isometric phase of contraction and accelerates during shortening, simulated here by increasing the value of k_6 from 4 to 10 s^{-1}, which causes force to decrease to 20% of its value before shortening. After the period of shortening, force redevelops and the ATPase decreases again to the value before shortening.

An explanation of the Fenn effect based on an acceleration of cross-bridge detachment was put forward by Potma et al. (1994) and is in accordance with the values of attachment and detachment rate constants in isometric conditions and during shortening (e.g., Brenner and Eisenberg, 1986). A strain-dependent change in the nucleotide affinity of the myosin also seems compatible with the present view on S1 atomic structure as discussed by Geeves and Holmes (1999).

Actin-myosin interaction kinetics in slow and fast 2A fibers

The high time resolution and sensitivity of the fluorescence method used here in isolated single fibers offer a unique opportunity to compare myosin isoforms in nearly physiological conditions and to precisely determine the distance traveled by a myosin head during each hydrolytic cycle (D_{ATP}) (Irving and Woledge, 1981; Irving, 1991; Higuchi and Goldman, 1991). All subsequent calculations were carried out under the assumption that the amplitude of the

working stroke (D_W), 10 nm, was the same in slow and fast myosin isoforms. Values of D_W reported in the literature vary according to the techniques used: ~5 nm from single-molecule studies (Veigel et al., 1998; Kitamura et al., 1999), 9 nm from T2 curves of isolated intact fibers (Goldman and Huxley, 1994), and even ~20 nm (Ishijima et al., 1996). No measurement of D_W in different skeletal muscle myosin isoforms is available, but evidence has been obtained that D_W in smooth myosins and that in skeletal myosins are identical (Guilford and Warshaw, 1998), as are D_W values in V1 and V3 cardiac myosins (Sugiura et al., 1998; Palmiter et al., 1999).

The assumption of a given value of D_W affects the calculation of the duty ratio (DR): if D_W is assumed to be 5 nm instead of 10 nm, the DR values become half of the values shown in Fig. 8. For example, at maximum shortening velocity the fraction of attached myosin heads will decrease from 7% to 3.5%. The aim of this study, however, is the comparison between myosin isoforms, and all conclusion reached are, therefore, independent of the actual amplitude of D_W.

Under the above assumptions slow fibers were found to travel for a longer distance during each ATP hydrolysis cycle (longer D_{ATP}) at all velocities and therefore to have a lower duty ratio (DR) than fast fibers (see Fig. 8, *A* and *B*). Fig. 10 *C* shows that using the parameters obtained by force-velocity fitting the model closely simulates the results reported in Fig. 8 *B*. On the other hand, the duty ratio was found to be equal when the two fiber types were compared at the same tension (see Fig. 8 *C*). The model also reproduces this result, as can be seen in Fig. 10 *D*. Thus the main difference between fast and slow fibers is that at each speed of shortening the fraction of attached myosin heads is higher in fast fibers. As the relation between the fraction of attached heads and tension is the same in fast and slow fibers, fast fibers are able to develop more tension at each speed and therefore more power. According to the model the fraction of attached myosin heads is greater in fast than in slow fibers because the rate constant of the ATP hydrolysis step is greater in fast fibers. This rate constant is the rate-limiting step of the ATPase cycle during shortening and controls the cross-bridge attachment in force-generating states (AM·ADP·P_i and AM·ADP). This is in general agreement with the conclusion reached by Zhao and Kawai (1994) and by Wang and Kawai (1997), who compared the responses of fast and slow rabbit fibers to oscillations at various frequencies. Their model shows that the main difference is in the steps preceding force development and identified in the ATPase cycle as P_i release and subsequent isomerization. The analysis of cross-bridge kinetics carried out by Barclay et al. (1993) and based on Huxley's (1957) model also implies that during shortening the fraction of attached bridges is greater in fast than in slow fibers, as the attachment rate constant f_1 is five times higher in fast than in slow fibers, whereas the detachment rate constant g_2 is only two times greater. Interestingly, recent single-molecule studies suggest that the diversity is mainly localized in the detachment rate (Sugiura et al., 1998; Palmiter et al., 1999). This might be explained by assuming that (at variance with the conditions of the single-molecule studies) in a fiber during active shortening, the detachment rate (or the ADP release rate, which in the model controls the detachment rate) is mainly controlled by the strain and load conditions.

Temperature effect on actin-myosin interactions and force generation

The present results and the model analysis contribute to an understanding of the effect of temperature. The increase in duty ratio with temperature at any given velocity of shortening is consistent with the view that the fraction of cross-bridges, which are attached to the thin filaments in a stereospecific manner and are generating force, increases with temperature. Temperature jump experiments on frog muscle fibers during contraction (Tsaturyan et al., 1999) have shown that the increase in force observed with increases in temperature is accompanied by an enhancement of the intensity of the first actin layer line in the x-ray diffraction pattern, consistent with cross-bridge labeling of the actin helix (Huxley et al., 1981). However, the present findings also suggest that force per myosin cross-bridge increases with increasing temperature (Fig. 8, *C* and *D*). An increase in force per myosin head is also suggested by the observation that the increase in force with temperature overcomes the increase in stiffness (Zhao and Kawai, 1994). In conclusion, the well-known increase in force after an increase in temperature is likely to depend on an increase in the fraction of myosin heads that are attached in a force-bearing state and on an increase in the force generated by individual myosin heads. Interestingly, the effect of temperature on the force generated by a myosin head is the same for slow and fast 2A myosins (Fig. 8, *C* and *D*). The model analysis fully supports the above interpretation, as the experimental results could be reproduced with two assumptions: 1) the rate constants are doubled, and this allows us to increase the fraction of attached myosin heads at each speed of shortening (see Fig. 10, *C* and *D*), and 2) the force coefficient is increased by 1.5, and this accounts for the ability to develop tension with a lower duty ratio (see Fig. 10 *D*). That the force per attached myosin head increases by 1.5 with temperature is also indicated by Fig. 8 *D*.

Efficiency

This study reports the first determination of the thermodynamic efficiency of human muscle fibers in vitro. In addition to the interest for applied physiology, the present determination of the efficiency of the chemomechanical

transduction in fibers containing distinct myosin isoforms points to two important conclusions:

1. Despite the different physiological characteristics of slow and fast muscle fibers, their peak efficiencies are remarkably similar, in contrast to the nearly fourfold differences in the maximum mechanical power output and the ATP hydrolysis rate.

2. The peak efficiency increases with temperature in the range explored (12–20°C) as a direct effect of the higher thermal sensitivity of shortening velocity and mechanical power compared to that of the ATP consumption rate.

The similarity in peak efficiency between fast and slow fibers is in general agreement with our previous comparison between slow and fast 2B fibers in the rat (Reggiani et al., 1997). In that case, however, the efficiency of fast fibers was slightly lower than that of slow fibers. This might be related to the different type of fast fibers studied (2B in the rat and 2A in humans) or to the different species. By the same methods, the maximum efficiency of rabbit psoas fibers, which are likely to be type 2X (Aigner et al., 1993), was found to be 0.36 (He et al., 1999), a value higher than that found here for human muscle at the same temperature. Barclay et al. (1993) also concluded that the efficiency was similar in fast and slow intact mouse muscles, although mechanical instead of thermodynamic efficiency was determined, and the partition of the whole energy release between isometric and velocity-dependent components was very different. The conclusion that slow muscles had a higher mechanical efficiency than fast muscles was reached by previous studies based on heat measurements (Woledge, 1968; Gibbs and Gibson, 1972; Wendt and Gibbs, 1973). However, on the basis of energy utilization calculated from measurements of oxygen consumption, Heglund and Cavagna (1987) arrived at the opposite conclusion, i.e., that fast muscles have a higher efficiency than slow muscles.

Our observation that the maximum efficiency of shortening is similar in fibers containing fast and slow myosin isoforms is consistent with the view discussed above that if the amplitude of the working stroke is the same in slow and fast myosin, tension developed by a single interaction will also be the same. The difference between myosin isoforms is not in the fraction of ATP energy converted into mechanical work, but in the rate at which the energy conversion occurs. The sizes of the elementary displacement and tension are probably largely constrained by the structure of the myosin cross-bridge. On the other hand, the large differences in maximum and optimal shortening velocities between fibers containing slow and fast myosins is accounted for by differences in the kinetic parameters controlling cross-bridge cycling.

The absolute values of thermodynamic efficiency are dependent on the value of the energy content of ATP under the experimental conditions. As a first approximation a value of 50 kJ/mol was selected and used in this study (Kushmerick and Davies, 1969). During the contractile response that follows the caged ATP release the concentrations of ATP, ADP, and P_i inside the fiber are likely to be 1.5 mM, 0.2 mM, and 0.001 mM, respectively. This would lead to a value of ATP free energy at 12°C of 57.9 kJ/mol, if the standard ATP free energy is 36.8 kJ/mol (Alberty, 1969). With these assumptions the calculated efficiency shown in Figs. 5 and 7 should be reduced by ~15%. At 20°C the free energy of ATP, assuming the same concentrations of reactant and products, is 58.5 kJ/mol, so that the efficiency values at 20°C should be also reduced by ~15%. The overall effect of temperature is small and insufficient to explain the increase in efficiency with temperature. The increase in maximum efficiency with temperature is a direct consequence of the lower thermal sensitivity of the ATP hydrolysis rate compared to that of shortening velocity and mechanical power. The increase in efficiency can find a likely explanation in the temperature-dependent increase in the fraction of cross-bridges attached to actin in a force-bearing conformation (Tsaturyan et al., 1999).

Temperature effects may also be important in interpreting the differences in efficiency found in different studies. The effect of temperature on chemomechanical energy transduction may help us to understand why estimates of human muscle efficiency in vivo (at ~37°C) are different from the values obtained here. Mechanical power does not increase linearly with temperature (Ranatunga, 1998), so that our data cannot be extrapolated to physiological human muscle temperature. Determination of muscle efficiency in human muscles in situ is difficult, because mechanical and local metabolic conditions are hard to control. Estimated thermodynamic efficiencies range from 0.15 to 0.35 (Gaesser and Brooks, 1975; Ryschon et al., 1997), without correction for the energetic cost of excitation-contraction coupling or precise determination of the speed of the length change. With appropriate corrections to define the energy expenditure in the myofibrils, the efficiency of human muscles i*n situ* was estimated to reach 0.5 or higher (Gaesser and Brooks, 1975). The results obtained here appear to be fully compatible with those values.

We are grateful to Drs. M. R. Webb, M. Brune, and J. E. T. Corrie for the supply of phosphate-binding protein and MDCC; to Mr. R. K. Chillingworth for his help with the instrumentation; and to D. R. Trentham, FRS, for his help and advice throughout.

This work was supported by European Union grant CEC CHRX CT 94-0606, by a Cofinanziamento dei programmi di ricerca di interesse nazionale-1998 grant from the Ministero dell'Universita e della Ricerca Scientifica e Tecnologica (Italy), and by direct support from the Medical Research Council (UK).

REFERENCES

Aigner, S., B. Gohlsch, N. Hamalainen, R. S. Staron, A. Uber, U. Wehrle, and D. Pette. 1993. Fast myosin heavy chain diversity in skeletal muscles of the rabbit: heavy chain IId, not IIb predominates. *Eur. J. Biochem.* 211:367–372.

Alberty, R. A. 1969. Standard Gibbs free energy, enthalpy and enthropy changes as a function of pH and pMg for several reactions involving adenosine phosphates. *J. Biol. Chem.* 244:3290–3302.

Barclay, C. G., J. K. Constable, and C. L. Gibbs. 1993. Energetics of fast- and slow-twitch muscles of the mouse. *J. Physiol. (Lond.).* 472:61–80.

Biral, D., R. Betto, D. Danieli-Betto, and G. Salviati. 1988. Myosin heavy chain composition of single fibres from normal human muscle. *Biochem. J.* 250:307–308.

Bottinelli, R., M. Canepari, M. A. Pellegrino, and C. Reggiani. 1996. Force-velocity properties of human skeletal muscle fibres: myosin heavy chain isoform and temperature dependence. *J. Physiol. (Lond.).* 495: 573–586.

Bottinelli, R., M. Canepari, C. Reggiani, and G. J. M. Stienen. 1994. Myofibrillar ATPase activity during isometric contraction and isomyosin composition in rat single skinned muscle fibres. *J. Physiol. (Lond.).* 481:663–675.

Bottinelli, R., S. Schiaffino, and C. Reggiani. 1991. Force-velocity relations and myosin heavy chain isoform compositions of skinned fibres from rat skeletal muscle. *J. Physiol. (Lond.).* 437:655–672.

Brenner, B., and E. Eisenberg. 1986. Rate of force generation in muscle: correlation with actomyosin ATPase activity in solution. *Proc. Natl. Acad. Sci. USA.* 83:3542–3546.

Brune, M., J. L. Hunter, J. E. T. Corrie, and M. R. Webb. 1994. The direct, real-time measurement of rapid inorganic phosphate release using a novel fluorescent probe and its application to actomyosin subfragment 1. *Biochemistry.* 33:8262–8271.

Brune, M., J. L. Hunter, S. A. Howell, S. R. Martin, T. L. Hazlett, J. E. T. Corrie, and M. R. Webb. 1998. Mechanism of inorganic phosphate interaction with phosphate binding protein from *Escherichia coli*. *Biochemistry.* 37:10370–10380.

Chase, P. B., and M. J. Kushmerick. 1988. Effects of pH on contraction of rabbit fast and slow muscle fibers. *Biophys. J.* 53:935–946.

Corrie, J. E. T., Y. Katayama, G. P. Reid, M. Anson, and D. R. Trentham. 1992. The development and application of photosensitive caged compounds to aid time-resolved structure determination of macromolecules. *Philos. Trans. R. Soc. Lond. A.* 340:233–244.

Ferenczi, M. A., E. Homsher, and D. R. Trentham. 1984. The kinetics of magnesium adenosine triphosphate cleavage in skinned muscle fibres of the rabbit. *J. Physiol. (Lond.).* 352:575–599.

Gaesser, G. A., and G. A. Brooks. 1975. Muscular efficiency during steady-rate exercise: effects of speed and work rate. *J. Appl. Physiol.* 38:1132–1139.

Geeves, M. A., and K. C. Holmes. 1999. Structural mechanism of muscle contraction. *Ann. Rev. Biochem.* 68:687–728.

Gibbs, C. L., and W. R. Gibson. 1972. Energy production of rat soleus muscle. *Am. J. Physiol.* 223:864–871.

Goldman, Y. E. 1987. Kinetics of the actomyosin ATPase in muscle fibers. *Annu. Rev. Physiol.* 49:637–654.

Goldman, Y. E., and A. F. Huxley. 1994. Actin compliance: are you pulling my chain? *Biophys. J.* 67:2131–2136.

Guilford, W. H., and D. M. Warshaw. 1998. The molecular mechanics of smooth muscle myosin. *Comp. Biochem. Physiol. B.* 119:451–458.

He, Z.-H., R. K. Chillingworth, M. Brune, J. E. T. Corrie, D. R. Trentham, M. R. Webb, and M. A. Ferenczi. 1997. ATPase kinetics on activation of permeabilized isometric fibers from rabbit and frog muscle: a real time phosphate assay. *J. Physiol. (Lond.).* 501:125–148.

He, Z.-H., R. K. Chillingworth, M. Brune, J. E. T. Corrie, M. R. Webb, and M. A. Ferenczi. 1999. The efficiency of contraction in rabbit skeletal muscle fibres, determined from the rate of release of inorganic phosphate. *J. Physiol. (Lond.).* 517.3:839–854.

He, Z.-H., R. K. Chillingworth, and M. A. Ferenczi. 1998b. The ATPase activity in isometric and shortening skeletal muscle fibers. *In* Mechanism of Work Production and Work Absorption in Muscle. H. Sugi and G. H. Pollack, editors. Plenum, New York. 331–341.

He, Z.-H., G. J. M. Stienen, J. P. F. Barends, and M. A. Ferenczi. 1998a. Rate of phosphate release after photoliberation of ATP in slow and fast skinned skeletal muscle fibers. *Biophys. J.* 75:2389–2401.

Heglund, N. C., and G. A. Cavagna. 1987. Mechanical work, oxygen consumption, and efficiency in isolated frog and rat muscle. *Am. J. Physiol.* 253:C22–C29.

Higuchi, H., and Y. E. Goldman. 1991. Sliding distance between actin and myosin filaments per ATP molecule hydrolysed in skinned muscle fibres. *Nature.* 352:352–354.

Holroyd, S. M., C. L. Gibbs, and A. R. Luff. 1996. Shortening heat in slow- and fast-twitch muscles of the rat. *Am. J. Physiol.* 270:C293–C297.

Horiuti, K., N. Yagi, and S. Takemori. 1997. Mechanical study of rat soleus muscle using caged ATP and X-ray diffraction: high ADP affinity of slow cross-bridges. *J. Physiol. (Lond.).* 502:433–447.

Huxley, A. F. 1957. Muscle structure and theories of contraction. *Prog. Biophys. Biophys. Chem.* 7:255–318.

Huxley, H. E., R. M. Simmons, A. R. Faruqi, M. Kress, J. Bordas, and M. H. Koch. 1981. Millisecond time-resolved changes in x-ray reflections from contracting muscle during rapid mechanical transients, recorded using synchrotron radiation. *Proc. Natl. Acad. Sci. USA.* 78: 2297–2301.

Irving, M. 1991. Motor proteins. Biomechanics goes quantum. *Nature.* 352:284–286.

Irving, M., and R. C. Woledge. 1981. The dependence on extent of shortening of the extra energy liberated by rapidly shortening frog skeletal muscle. *J. Physiol. (Lond.).* 321:411–422.

Ishijima, A., H. Kojima, H. Higuchi, Y. Harada, T. Funatsu, and T. Yanagida. 1996. Multiple- and single-molecule analysis of the actomyosin motor by nanometer-piconewton manipulation with a microneedle: unitary steps and forces. *Biophys. J.* 70:383–400.

Kitamura, K., M. Tokunaga, A. H. Iwane, and T. Yanagida. 1999. A single myosin head moves along an actin filament with regular steps of 5.3 nanometres. *Nature.* 397:129–134.

Kushmerick, M. J., and R. E. Davies. 1969. The chemical energetics of muscle contraction. II. The chemistry, efficiency and power of maximally working sartorius muscles. *Proc. R. Soc. Lond. B.* 174:315–353.

Laemmli, U. K. 1970. Cleavage of structural proteins during the assembly of the head of bacteriophage T4. *Nature.* 227:680–685.

Larsson, L., and R. L. Moss. 1993. Maximum velocity of shortening in relation to myosin isoform composition in single fibres from human skeletal muscles. *J. Physiol. (Lond.).* 472:595–614.

Lauzon, A. M., M. J. Tyska, A. S. Rovner, Y. Freyzon, D. M. Warshaw, and K. M. Trybus. 1998. A 7-amino-acid insert in the heavy chain nucleotide binding loop alters the kinetics of smooth muscle myosin in the laser trap. *J. Muscle Res. Cell Motil.* 19:825–837.

Linari, M., I. Dobbie, M. Reconditi, N. Koubassova, M. Irving, G. Piazzesi, and V. Lombardi. 1998. The stiffness of skeletal muscle in isometric contraction and rigor: the fraction of myosin heads bound to actin. *Biophys. J.* 74:2459–2473.

Linari, M., and R. C. Woledge. 1995. Comparison of energy output during ramp and staircase shortening in frog muscle fibers. *J. Physiol. (Lond.).* 487:699–710.

Palmiter, K. A., M. J. Tyska, D. E. Dupuis, N. R. Alpert, and D. M. Warshaw. 1999. Kinetic differences at the single molecule level account for the functional diversity of rabbit cardiac myosin isoforms. *J. Physiol. (Lond.).* 519:669–678.

Pate, E., K. Franks-Skiba, and R. Cooke. 1998. Depletion of phosphate in active muscle fibers probes actomyosin states within the powerstroke. *Biophys. J.* 74:369–380.

Potma, E. J., and G. J. M. Stienen. 1996. Increase in ATP consumption during shortening in skinned fibers from rabbit psoas muscle: effects of inorganic phosphate. *J. Physiol. (Lond.).* 496:1–12.

Potma, E. J., G. J. M. Stienen, J. P. Barends, and G. Elzinga. 1994. Myofibrillar ATPase activity and mechanical performance of skinned fibres from rabbit psoas muscle. *J. Physiol. (Lond.).* 474:303–317.

Potma, E. J., I. A. van Grass, and G. J. M. Stienen. 1995. Influence of inorganic phosphate and pH on ATP utilization in fast and slow skeletal muscle fibers. *Biophys. J.* 69:2580–2589.

Ranatunga, K. W. 1998. Temperature dependence of mechanical power output in mammalian (rat) skeletal muscle. *Exp. Physiol.* 83:371–376.

Reggiani, C., E. J. Potma, R. Bottinelli, M. Canepari, M. A. Pellegrino, and G. J. M. Stienen. 1997. Chemo-mechanical energy transduction in relation to myosin isoform composition in skeletal muscle fibers of the rat. *J. Physiol. (Lond.).* 502:449–460.

Reiser, P. J., R. L. Moss, G. G. Giulian, and M. L. Greaser. 1985. Shortening velocity in single fibers from adult rabbit soleus muscles is correlated with myosin heavy chain composition. *J. Biol. Chem.* 260: 9077–9080.

Ryschon, T. W., M. D. Fowler, R. E. Wysong, A. Anthony, and R. S. Balaban. 1997. Efficiency of human skeletal muscle in vivo: comparison of isometric, concentric, and eccentric muscle action. *J. Appl. Physiol.* 83:867–874.

Smerdu, V., I. Karsch-Mizrachi, M. Campione, L. Leinwand, and S. Schiaffino. 1994. Type IIx myosin heavy chain transcripts are expressed in type IIb fibers of human skeletal muscle. *Am. J. Physiol.* 267: C1723–C1728.

Stienen, G. J. M., R. Bottinelli, J. Kiers, and C. Reggiani. 1996. Myofibrillar ATPase activity in skinned human skeletal muscle fibers: fiber type and temperature dependence. *J. Physiol. (Lond.).* 493:299–307.

Sugiura, S., N. Kobayakawa, H. Fujita, H. Yamashita, S. Momomura, S. Chaen, M. Omata, and H. Sugi. 1998. Comparison of unitary displacements and forces between two cardiac myosin isoforms by the optical trap technique: molecular basis for cardiac adaptation. *Circ. Res.* 82: 1029–1034.

Thirlwell, H., J. E. T. Corrie, G. P. Reid, D. R. Trentham, and M. A. Ferenczi. 1994. Kinetics of relaxation from rigor of permeabilized fast-twitch fibers from the rabbit using a novel caged ATP and apyrase. *Biophys. J.* 67:2436–2447.

Tsaturyan, A. K., S. Y. Bershitsky, R. Burns, and M. A. Ferenczi. 1999. Structural changes in the actin-myosin cross-bridges associated with force generation induced by temperature jump in permeabilized frog muscle fibers. *Biophys. J.* 77:354–372.

Veigel, C., M. L. Bartoo, D. C. White, J. C. Sparrow, and J. E. Molloy. 1998. The stiffness of rabbit skeletal actomyosin cross-bridges determined with an optical tweezers transducer. *Biophys. J.* 75:1424–1438.

Wang, G., and M. Kawai. 1997. Force generation and phosphate release steps in skinned rabbit soleus slow-twitch muscle fibers. *Biophys. J.* 73:878–894.

Wendt, I. R., and C. L. Gibbs. 1973. Energy production of rat extensor digitorum longus muscle. *Am. J. Physiol.* 224:1081–1086.

Widrick, J. J., S. W. Trappe, D. L. Costill, and R. H. Fitts. 1996. Force-velocity and force-power properties of single muscle fibers from elite master runners and sedentary men. *Am. J. Physiol.* 271:C676–C683.

Woledge, R. C. 1968. The energetics of tortoise muscle *J. Physiol. (Lond.).* 197:685–707.

Zhao, Y., and M. Kawai. 1994. Kinetic and thermodynamic studies of the cross-bridge cycle in rabbit psoas muscle fibers. *Biophys. J.* 67: 1655–1668.